He *et al. Biochar* (2025) 7:88
https://doi.org/10.1007/s42773-025-00465-z

Biochar

ORIGINAL RESEARCH

Open Access

Conversation of pesticide residues into ammonium nitrogen (NH_4^+-N) through AOPs and its fertilization effect on lettuce growth

Dong He[1,2†], Yujiao Wen[1,2†], Shangzhi Wei[3], Shikai Li[4], Lide Liu[1,2], Jinmeng Wu[1,2], Zhi Zhou[1,2], Nan Zhou[1,2*], Hongmei Liu[1,2*] and Zhonghua Zhou[1,2*]

Abstract

Eliminating pesticide residues in soil through the Advanced Oxidation Processes (AOPs) has been attracted a lot of attention in recent years. However, the potential of converting them into small molecular nutrients such as ammonium nitrogen (NH_4^+-N) has been significantly ignored. Herein, we systematically detected the transformation of clothianidin (CTD) into NH_4^+-N through AOPs and the following effect on the growth of lettuce. Fe_3S_4-loaded biochar (BC@Fe_3S_4) was synthesized in one step through hydrothermal method, possessing excellent catalytic capacity to activate peroxymonosulfate (PMS). The results showed that the generated NH_4^+-N could reach up to 3.029 mg L^{-1} in soil–water system containing 20 mg L^{-1} of CTD after the treatment of BC@Fe_3S_4 + PMS. However, when the concentration of CTD in soil was 20 mg kg^{-1}, the dry weight of lettuce was 17.3 mg/plant, and the dry weight of lettuce in CTD-contaminated soil with this concentration was 29.3 mg/plant after treatment by BC@Fe_3S_4 + PMS, and no CTD residue was detected. The results of lettuce cultivation showed that CTD in the system was converted to NH_4^+-N after treatment with BC@Fe_3S_4 + PMS, which resulted in increased dry matter accumulation and decreased residue of lettuce seedlings. Meanwhile, LC–MS/MS analysis revealed three main degradation routes involved in the CTD degradation process. T.E.S.T-QSAR was carried out to simulate the toxicity of all degradation intermediates to Fathead minnow and T.pyriformis, manifesting that the CTD toxicity decreased after BC@Fe_3S_4 + PMS treatment. Further analysis indicated that the degradation of CTD and the formation of NH_4^+-N occurred simultaneously, where •OH, $^1O_2$ and $SO_4^{\bullet-}$ played a leading role in trigging those reactions. This work explains in detail the mechanism by which pesticides are converted into nutrients, providing feasible strategies and new perspectives for soil remediation.

Highlights

- Soil-bound CTD could be transformed into NH_4^+-N through BC@Fe_3S_4–AOPs system.
- CTD degradation products could provide nutrients and promote the growth of lettuce.

†Dong He and Yujiao Wen contributed equally to this work.

*Correspondence:
Nan Zhou
zhounan@hunau.edu.cn
Hongmei Liu
liuhongmei@hunau.edu.cn
Zhonghua Zhou
zhouzhonghua1976@hotmail.com
Full list of author information is available at the end of the article

Springer

© The Author(s) 2025. **Open Access** This article is licensed under a Creative Commons Attribution 4.0 International License, which permits use, sharing, adaptation, distribution and reproduction in any medium or format, as long as you give appropriate credit to the original author(s) and the source, provide a link to the Creative Commons licence, and indicate if changes were made. The images or other third party material in this article are included in the article's Creative Commons licence, unless indicated otherwise in a credit line to the material. If material is not included in the article's Creative Commons licence and your intended use is not permitted by statutory regulation or exceeds the permitted use, you will need to obtain permission directly from the copyright holder. To view a copy of this licence, visit http://creativecommons.org/licenses/by/4.0/.

- •OH, $^1O_2$ and $SO_4^{\bullet-}$ played an important role in the BC@Fe_3S_4 + PMS + CTD system.
- It is feasible to remove soil pesticides and replenish nitrogen simultaneously.
- BC@Fe_3S_4 + PMS is a potential soil remediation technology.

Keywords Nutrient conversion, Advanced oxidation process, Biochar, Soil remediation, Free radical, Neonicotinoid pesticides

Graphical Abstract

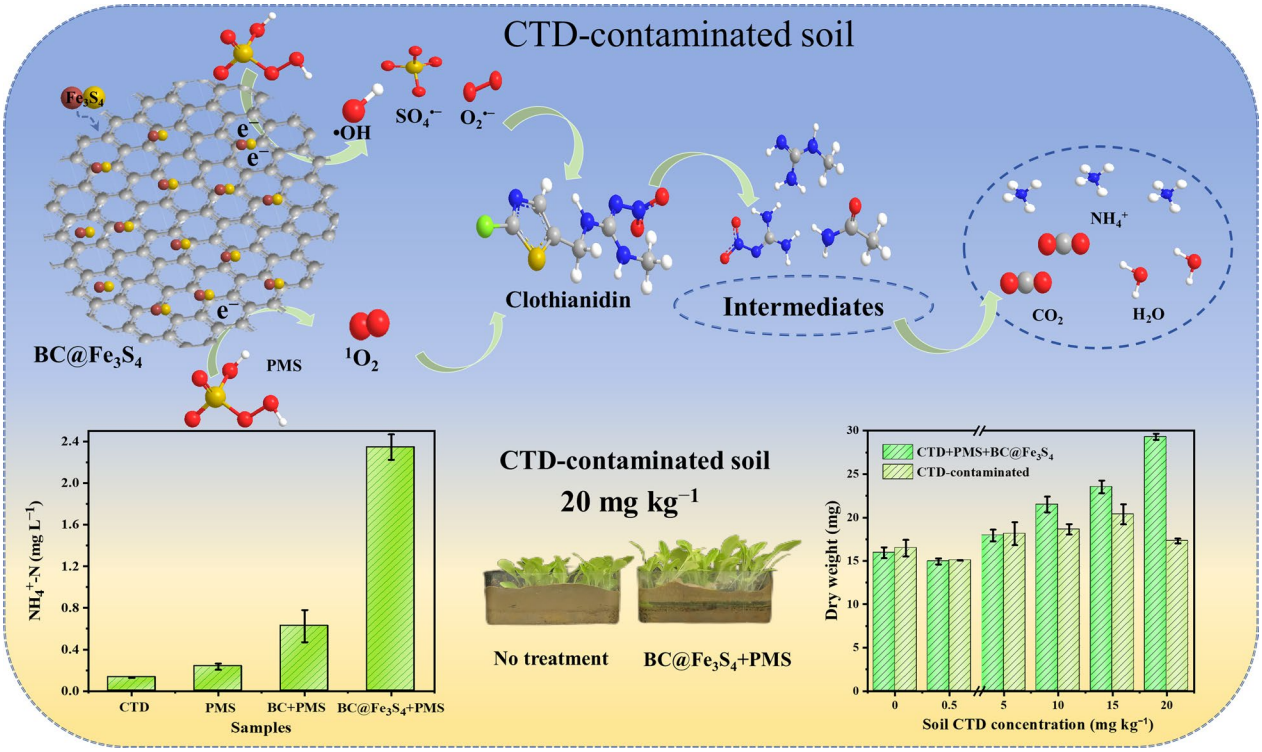

1 Introduction

With the accumulation of population, the pesticide was widely used to get high-yield and quality crops (Wood and Goulson 2017). However, the overuse of pesticides, driven by a lack of scientific guidance, has introduced persistent organic pollutants (POPs) into the agricultural environment. These POPs linger in the soil, threatening both human health and the ecosystem (Sandstrom et al. 2022). CTD is a new type of highly efficient and highly selective insecticide in the Neonicotinoids (NEOs), which has been widely used in pest control of rice, vegetables and other crops (Li et al. 2012; Tian et al. 2022). It has been reported that the content of CTD in agricultural soil is high, up to 0.002–2.06 mg kg^{-1} (Chowdhury et al. 2012; Jones et al. 2014), and the residual time is long, with a half-life of up to 148–6931 days (Wood and Goulson 2017). Relevant studies have shown that plants will absorb the CTD in the soil and accumulate in the plant, and people will eat vegetables with pesticide residues and they eventually enter the human body (Yang et al. 2022), posing a great threat to human health (Kalyabina et al. 2021). How to effectively remove organic insecticides such as clothianidin from the soil environment has become a challenge for researchers.

At present, AOPs are considered as a highly feasible approach to treat the contamination of pesticide in soil with both free radical and non-free radical pathways (Gupta et al. 2022; Wen et al. 2024). The AOPs system based on the joint action of persulfate and efficient catalysts can quickly generate reactive oxygen species (ROS) such as •OH, $SO_4^{\bullet-}$, $O_2^{\bullet-}$and $^1O_2$, and can transform stubborn organic pollutants into low-toxic and non-toxic substances (Ebrahimi et al. 2021). Notably, a large number of studies have confirmed that catalysts play a very important role in AOPs (Alamgholiloo et al. 2021). At present, the main catalysts include transition metals and their oxides, hydroxides, sulfides and metal–organic frameworks and others (Taghavi et al. 2022). Among them, transition metals have received more and more attention in the removal of organic pollutants due to their economy and high REDOX properties (Li et al. 2022a; Manjuri Bhuyan et al. 2023). However, despite the excellent catalytic properties of transition metals, they still face some challenges in practical applications, such as poor dispersion of catalysts and easy aggregation and inactivation of active sites. Therefore, loading the transition metal on a suitable carrier can not only improve its dispersion and stability, but also enhance its application performance in complex environments. Biochar-based materials have been widely studied as catalyst carriers in AOPs applications because of their advantages such as controllable activation degree, high conversion efficiency and simple structure (Li et al. 2022b; Wang et al. 2022). Therefore, it is expected to remove organic pollutants in the actual agricultural environment by synthesizing a composite material with biochar as the carrier and transition metal compounds on it. Unfortunately, numerous rstudies have confirmed that the degradation of pesticide by AOPs cannot mineralize completely, leading to the generation of abundant intermediates, which produce beneficial and/or harmful components during degradation, and these intermediates are often ignored during the degradation process (Bandeira et al. 2021; Mohanta and Ahmaruzzaman 2020). Herein, there is an urgent need to determine the environmental impact of the resulting intermediates in order to make efficient use of the beneficial components produced during degradation.

Notably, many of the typical pesticides such as insecticides, herbicides, antibiotics and so on are rich in N, P, S and other nutrients (Chen et al. 2019; Wen et al. 2022). which might be converted into nutrients that can be absorbed by crops (Marcińczyk et al. 2022). There are several studies (Chen et al. 2023; Guo et al. 2021; Jin et al. 2024; Wen et al. 2022) showing that intermediates related to nitrate, phosphate and organic acid may be obtained during the degradation of Sulfamethazine ($C_6H_9N_3O_2S$), Glyphosate ($C_3H_8NO_5P$) and Clothianidin ($C_6H_8ClN_5O_2S$),etc. Besides, ROS can attack some heterocycles and benzoquinones containing S or N to destroy their N–C and S-C bonds, getting S and N containing small molecules. Above small molecules could be oxidized to get free ammonium salts (NH_4^+), nitrate nitrogen (NO_3^-) (Guo et al. 2021) and other beneficial products (Li et al. 2022a), promoting the growth of plants. Unfortunately, the specific mechanisms of getting nutrients degraded from pesticides and the effects of the pesticides into nutrients on crops are unclear. Therefore, it is particularly important to study the remediation of soil organic pollution by AOPs, the mechanism of pollutant conversion into nutrients, and the impact on crop growth (Fatima et al. 2021; Hou et al. 2022; Kalyabina et al. 2021; Zou et al. 2022). NEOs, accounting for more than 30% of the global pesticide market (Wang et al. 2023), have been registered and used by more than 120 countries (Tu et al. 2023). Particularly, NEOs are rich in nitrogen. For example, Clothianidin (CTD), which accounts for 14.7% of total NEOs insecticide sales, has a nitrogen content of 22.43%. On the other hand, CTD residues have been frequently detected in various vegetables (Zhang et al. 2019), which have exceeded the concentration of CTD residues in food specified by the United States Environmental Protection Agency (0.01 mg kg^{-1}). Therefore, the removal of CTD in the soil environment is particularly important.

Based on the previous research results of our research group, a low-cost and environmentally friendly Iron and sulfur-modified biochar material was synthesized by hydrothermal method (Gao et al. 2022a). PMS was selected as the oxidant and nitrogen-containing CTD was selected as the typical pesticide. A maximum concentration of 200 mg kg^{-1} was set for contaminated soil to ensure a response when certain extreme concentrations occurred. Through a series of experiments and characterization, the properties and transformation mechanism of the materials were investigated. A new idea of repairing pesticide residues and nutrient conversion was put forward. The specific projects of this study are as follows: The residual CTD in the soil was decomposed into NH_4^+-N during the degradation process; CTD nutrient conversion products can provide nutrients and promote lettuce growth; ROS such as •OH, $^1O_2$ and $SO_4^{\bullet-}$ plays an important role in the BC@Fe_3S_4 + PMS + CTD system; The intermediates were identified by LC–MS/MS, and the toxicity evaluation software (T.E.S.T-QSAR) was used to simulate the toxicity changes of the intermediates; A new technique for removing soil organic pesticides and replenishing nitrogen at the same time was proposed; The experiment of lettuce culture confirmed that BC@Fe_3S_4 + PMS is a promising agricultural soil remediation technology.

2 Experiments

2.1 Materials and chemicals

All chemicals are purchased directly and are not further purified, as detailed in Supplemental information (SI) Text S1.

2.2 Preparation and characterization of BC@Fe_3S_4 and BC

The biomass came from Camellia oleifera shell base of Hunan Agricultural University. First, the camellia oleifera shell was cleaned with ultra-pure water, dried, and crushed after 100 mesh sieves (particle size is about 150 μm). Secondly, weighed 5.000 g camellia oleifera shell and then measured 25 mL thiourea with a concentration of 0.5 M, followed by ultrasound for 20 min, and then 20 mL of ferric chloride with a concentration of 0.72 M and 5 mL of sodium hydroxide with a concentration of 0.75 M were added successively. The precursor was obtained by stirring with a magnetic stirrer for 4 h. Finally, the precursor was put into a hydrothermal reaction axe, pyrolyzed at 200 ℃ for 16 h, and then washed under ultrasonic waves with a mixture of 1: 1 ethanol and water for 10 min. Subsequently, the sample was washed with ultra-pure water until pH became neutral, and dried at 60 ℃ for 5 h to obtain BC@Fe_3S_4. BC was prepared by replacing all the reagents with ultra-pure water according to the preparation method of BC@Fe_3S_4. BC@Fe_3S_4 and BC are characterized in Text S2. In this study, BC@Fe_3S_4 and BC were characterized by X-ray diffraction (XRD), Brunauer Emmett Teller (BET), scanning electron microscopy (SEM), energy dispersion spectroscopy (EDS), Fourier transform infrared spectrum (FT-IR), X-ray photoelectron spectroscopy (XPS), thermogravimetric analyzer (TGA), etc., and the specific methods and instruments are shown in Text S2. At the same time, electrochemical tests such as cyclic voltammetry (CV), electrochemical impedance spectroscopy (EIS), linear sweep voltammetry (LSV) were conducted on BC@Fe_3S_4 and BC, and the testing methods and details are shown in Text S3.

2.3 Soil sample treatment

The soil used in the experiment was taken from Yunyuan, Hunan Agricultural University. The preparation process of the soil contaminated by CTD was two steps, namely, the preparation of healthy soil and contaminated soil. First of all, the obtained fresh soil was completely dried, hammered fine, and then passed through a 100-mesh sieve to obtain a number of healthy soils with uniform thickness. Then, the 1.0 kg healthy soil and 206.1856 mg CTD were accurately weighed, and the CTD was dissolved in some ethanol, and then mixed according to the ratio of ethanol to soil 5: 1, and placed in the fume hood, during which the soil was fully stirred, dried, and hammered to obtain 200 mg kg^{-1} CTD contaminated soil. The physical and chemical properties of metal content, electric conductivity, organic carbon, pH and other properties of CTD-contaminated soil and fresh soil are shown in Tables.S1 and Tables.S2.

2.4 Nutrient conversion experiment of CTD

The effects of catalyst dosage (0.8, 1.6, 2.4, 3.2, 4.0 g kg^{-1}), PMS (0.8, 1.6, 2.4, 3.2, 4.0 mM), initial pH (2, 4, 6, 8, 10), CTD concentration (50, 100, 150, 200 mg kg^{-1}), temperature (288.15, 298.15, 308.15 K) and catalyst types on NH_4^+-N generation in the degradation system were investigated by single-factor experiments. The automatic multi-parameter flow injection analyzer (Model: iFIA7, Beijing Jitian Instruments Co.) was used in this experiment to measure NH_4^+-N. Refer to Text S4 for specific test methods and means. The optimum nutrient conversion conditions and the optimum degradation conditions were determined.

2.5 Greenhouse lettuce cultivation experiment

In this study, greenhouse lettuce cultivation experiments were conducted according to the methods reported in the literature (Yang et al. 2022). The test seeds will be disinfected and set aside. Each group of 20 seeds had 3 replicates. Different concentrations of CTD contaminated soil (0, 0.5, 5, 10, 15, 20 mg kg^{-1}) were set up. Of the two groups of treatment, one was CTD-contaminated group (without adding PMS and BC@Fe_3S_4), the other was CTD + PMS + BC@Fe_3S_4 system. The soil mass used in the two groups was 200.00 g. The CTD + PMS + BC@Fe_3S_4 system was treated according to the best scheme explored in this study (3.2 mM PMS, 2.4 g kg^{-1} BC@Fe_3S_4).

After adding the above substances, the germinating box was placed at 25℃ for 36 h, during which it was stirred evenly to make its chemical substances fully react, and then used for lettuce cultivation test. Lettuce seeds were planted in a sprouting box and then placed in a greenhouse. The same volume of water was added each time, keeping the water level consistent. Greenhouse conditions were as follows: temperature 20 ℃, photoperiod 12/12 h, relative humidity 65%, light intensity set to 12,000 Lux, to simulate the natural light source. Three lettuce seedlings were randomly selected from each bud box. The growth of lettuce roots and leaves was analyzed with WSEENLA-S plant root scanner, and the fresh and dry weight of lettuce was analyzed by electronic weighing. Methods for extraction and determination of CTD residues in soil and lettuce are shown in Text S5.

2.6 Degradation test for CTD

The degradation process of CTD by various catalysts and the degradation optimization experiment were carried out according to 2.4 Nutrient conversion experiment of CTD. The specific implementation process is shown in Text S6, while the extraction method of residual CTD and intermediates in soil is shown in Text S7.

2.7 Other analytical methods

The residual CTD concentration in the soil was determined by HPLC, the degradation intermediates of each system were identified by UHPLC-Q-TOF/MS, the main free radical types were detected in the electronic spin resonance (ESR) detection system, the mineralization efficiency of CTD was determined by total organic carbon (TOC) analyzer, and the heavy metal content in the soil was determined by FAAS. See Text S8 for the specific detection procedures. At the same time, the toxicity assessment software (T.E.S.T-QSAR) was used to simulate the toxicity changes of the intermediates (Text S9).

3 Results and discussion

3.1 Characterization of BC@Fe_3S_4

The surface morphology, elemental composition and distribution, crystal structure, functional group type, pore structure, electron transport ability and thermal stability of BC@Fe_3S_4 and BC catalysts were tested by SEM, EDS, XRD, FT-IR, BET, CV, EIS, LSV, TGA and other characterization instruments or methods. The results obtained are shown in Fig. S1-Fig. S4 and Table S3. Through the analysis of the characterization results, the following conclusions can be drawn: (1) The one-step hydrothermal carbonization method could make C, N, O, S, Fe and other elements uniformly distributed on the surface of BC@Fe_3S_4, and BC@Fe_3S_4 was modified by rich functional groups such as OH, C–O–C and the active component (Fe_3S_4). This makes BC@Fe_3S_4 had stronger catalytic activity and hydrophilicity, which is conducive to the catalytic reaction. (2) Compared with BC, it can be found that BC@Fe_3S_4 had a larger specific surface area of S_{BET} and BJH, which means that BC@Fe_3S_4 had more active sites and greater catalytic potential. At the same time, the results of electrochemical tests confirmed that BC@Fe_3S_4 had stronger REDOX and better electron transport ability. It can be seen that BC@Fe_3S_4 had better electrochemical performance, which provided a possibility for BC@Fe_3S_4 to catalyze the degradation of CTD by PMS. See Text S10 for a detailed reasoning of the above conclusions.

3.2 Evaluation of nutrient conversion and degradation performance of CTD

3.2.1 BC@Fe_3S_4 nutrition converts CTD to produce NH_4^+-N

To determine the conversion potential of CTD into fertilizer, the formation rate of NH_4^+-N within 2 h was examined, using BC@Fe_3S_4 as catalyst and PMS as oxidant. For comparison, pristine BC and pure PMS were employed as the counterparts. As shown in Fig. 1a, when CTD concentration in polluted soil was 200 mg kg^{-1}, the as-obtained NH_4^+-N content in CTD, PMS + CTD and BC + PMS + CTD system was 0.131 mg L^{-1}, 0.236 mg L^{-1} and 0.625 mg L^{-1}, respectively. At the meantime, the value of NH_4^+-N concentration in system BC@Fe_3S_4 + PMS + CTD can be up to 2.346 mg L^{-1}, indicating this system had excellent nutrient conversion property for CTD. Previous studies have shown that biochar can degrade many organic pesticides in the environment through catalytic activation of PMS (Diao et al. 2021; Ding et al. 2021). This confirms the potential of biochar catalysts for the degradation and conversion of CTD into nutrients, especially BC@Fe_3S_4 + PMS system, which can efficiently convert CTD to NH_4^+-N. In this study, several important parameters of BC@Fe_3S_4 + PMS + CTD system were optimized, and the source of excellent nutrient conversion ability of BC@Fe_3S_4 + PMS was further clarified.

Firstly, in order to evaluate the ability of BC@Fe_3S_4 + PMS system to convert residual CTD in soil to NH_4^+-N with different concentrations, four soil CTD concentrations (50, 100, 150, 200 mg kg^{-1}) were set in this study. Water: Soil = 10: 1, that is, the concentration of CTD in the soil and water mixture was (5, 10, 15, 20 mg L^{-1}), respectively. The results are shown in Fig. 1b. With CTD concentration of 5, 10, 15, and 20 mg L^{-1}, the NH_4^+-N produced by BC@Fe_3S_4 + PMS after 2 h treatment was 1.194 mg L^{-1}, 1.575 mg L^{-1},1.995 mg L^{-1}, and 2.432 mg L^{-1}, respectively. It can be seen that NH_4^+-N production increased with the increase of residual CTD concentration in soil. It can be found that BC@Fe_3S_4 + PMS system had a very good nutrient conversion effect on residual CTD in soil. In the next test, 200 mg kg^{-1} was used as the simulated soil polluted by CTD.

Subsequently, the effects of the dosage of BC@Fe_3S_4 (0.8, 1.6, 2.4, 3.2, 4.0 g kg^{-1}) on the conversion of CTD to NH_4^+-N in BC@Fe_3S_4 + PMS + CTD system were investigated. The results are shown in Fig. 1c. When the catalyst dosage was set to 0.8, 1.6, 2.4, 3.2, 4.0 g kg^{-1}, the NH_4^+-N in the system was found to be 2.136, 2.316, 2.562, 2.395 and 2.387 mg L^{-1}, respectively, after reaction for 2 h with each catalyst dosage. The possible reason for the above difference is that the increase in the amount of catalyst promotes the production of active substances (Duan et al. 2020), thus improving the efficiency of the conversion of

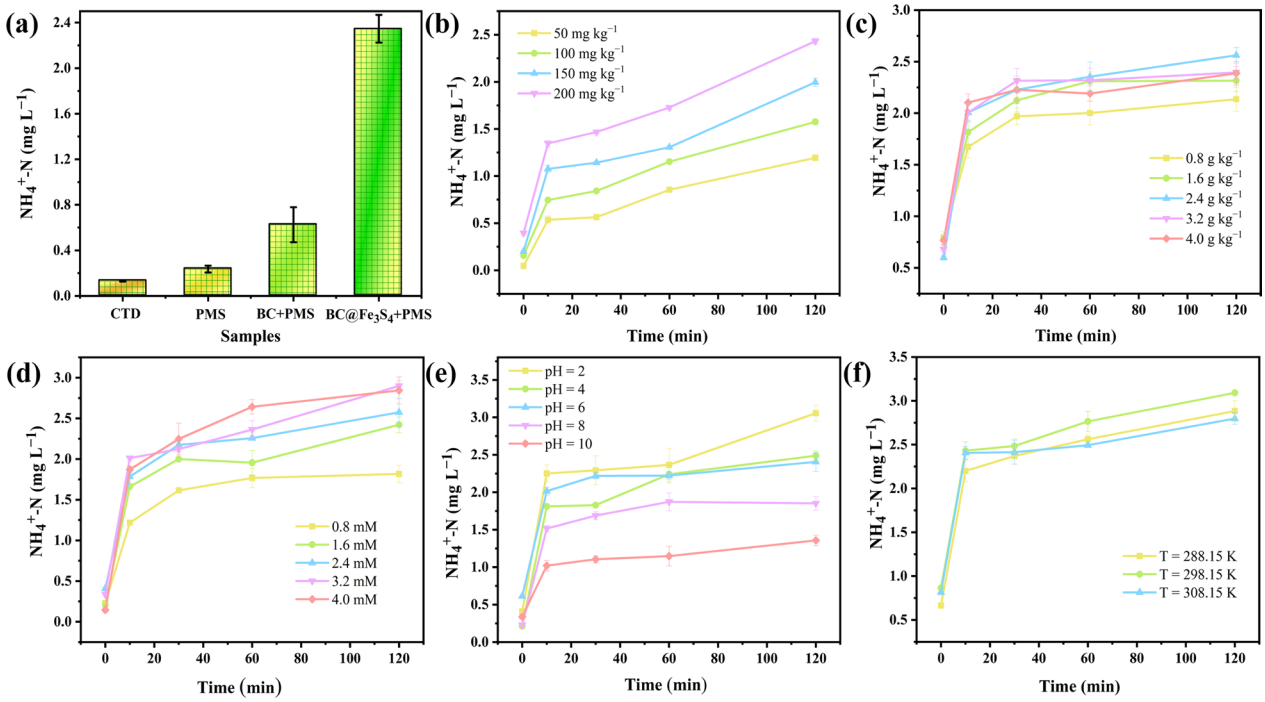

Fig. 1 NH_4^+-N generation in different environments. **a** catalyst, **b** CTD-concentrations, **c** BC@Fe_3S_4 dosage, **d** PMS concentrations, **e** pH, **f** Temperature. Test environment: all the above experiments were carried out in CTD-contaminates the soil. Reaction time = 2h, CTD-contaminates soil = 5.00 g, aqueous volume = 50 mL, catalyst dosage = 1.6 g kg^{-1}, [CTD] = 200 mg kg^{-1}, [PMS] = 3.2 mM, pH = No adjustment, T = 298.15 K. Due to space constraints when drawing figure, some abbreviations are used in Fig. 1, which are explained below. CTD: Soil contaminated by CTD; PMS: Adding PMS to CTD-contaminated soil; BC + PMS: Adding BC and PMS to CTD-contaminated soil; BC@Fe_3S_4 + PMS: BC@Fe_3S_4 and PMS are added to CTD-contaminated soil.

CTD to NH_4^+-N (Chen et al. 2019). When the dosage was greater than 1.6 g kg^{-1}, the NH_4^+-N generation efficiency was not significantly improved. From the perspective of cost control, the catalyst dosage of 1.6 g kg^{-1} was adopted in the subsequent experiment.

In order to clarify the effect of oxidant on the nutrient conversion of CTD, the effects of different concentrations of PMS (0.8–4.0 mM) on the conversion of CTD to NH_4^+-N were investigated. As shown in Fig. 1d, when the reaction time was 2 h and the PMS concentration increased from 0.8 mM to 2.4 mM, the conversion rate of NH_4^+-N increased from 1.817 mg L^{-1} to 2.575 mg L^{-1}. When PMS concentration was 3.2 mM and 4.0 mM, NH_4^+-N yield was 2.899 mg L^{-1} and 2.844 mg L^{-1}, respectively. Obviously, when the concentration of PMS was in the range of 0.8–3.2 mM, the generation of NH_4^+-N increased with the increase of the concentration of PMS. However, when the addition of PMS increased to 4.0 mM, the production of NH_4^+-N did not continue to increase. The possible reason is that the increase of PMS concentration will promote the generation of ROS, thereby improving the conversion efficiency of CTD. However, when the PMS concentration further increases, self-quenching phenomenon is prone to occur, resulting in the waste and loss of PMS (Fan et al. 2014; Ren et al. 2021). Therefore, the PMS concentration of 3.2 mM was selected as the best PMS dosage for subsequent experiments.

Since soil pH values are usually weakly acidic, neutral and weakly alkaline, in order to better evaluate the adaptability of BC@Fe_3S_4 + PMS in different application environments, different initial pH values (2, 4, 6, 8, 10) were set in this study to determine the influence of pH on the conversion of CTD to NH_4^+-N. As shown in Fig. 1e, when pH = 2, the generation of NH_4^+-N was 3.056 mg L^{-1}, while when pH = 10, the yield of NH_4^+-N decreased to 1.357 mg L^{-1}. It can be found that the NH_4^+-N generation efficiency in BC@Fe_3S_4 + PMS + CTD system under acidic conditions was significantly higher than that in alkaline environment. The results show that BC@Fe_3S_4 + PMS system could convert CTD into NH_4^+-N in both alkaline and acidic environments, and had strong adaptability. Meanwhile, in the process of soil restoration, the atmospheric temperature is around 298.15 K for most of the time, but the influence of temperature fluctuation on BC@Fe_3S_4 + PMS system should also be considered in the study, so the temperature range of 288.15 K–308.15 K

was set. The results are shown in Fig. 1f. When the ambient temperatures were 288.15 K, 298.15 K and 308.15 K respectively, within 2 h, the concentrations of CTD converted to NH_4^+-N were 2.884, 3.029 and 2.797 mg L^{-1}, respectively. This shows that BC@Fe_3S_4 + PMS + CTD system had strong adaptability to temperature, and it proves that BC@Fe_3S_4 + PMS had excellent anti-interference ability, which lays a foundation for its practical application.

3.2.2 Optimization of process conditions for CTD degradation by BC@Fe_3S_4

According to the above studies, it is evident that CTD can be transformed into NH_4^+-N. However, the extent to which BC@Fe_3S_4 + PMS can decompose CTD remains unclear. Therefore, it is particularly important to further evaluate the harmless degradation ability of BC@Fe_3S_4 + PMS for CTD. First, as shown in Fig. 2a, they were divided into four groups: PMS, BC, BC + PMS, BC@Fe_3S_4 + PMS. It was clear that BC@Fe_3S_4 + PMS could not only convert CTD into NH_4^+-N, but also degrade CTD completely in a short time. The results in Fig. 2b show that BC@Fe_3S_4 + PMS could remove 50 mg kg^{-1} CTD up to 100%, and the CTD concentration was 50 mg kg^{-1} in subsequent studies. Furthermore, the effects of different dosage of BC@Fe_3S_4 (0.8, 1.6, 2.4, 3.2, 4.0 g kg^{-1}) on CTD degradation were discussed, as shown in Fig. 2c. In the range of 0.8–4.0 g kg^{-1} catalyst, CTD degradation rate reached 100%. Follow-up studies were conducted using 0.8 g kg^{-1} BC@Fe_3S_4. The effects of different concentrations of PMS (0.8, 1.6, 2.4, 3.2, 4.0 mM) on the degradation system were subsequently investigated (Fig. 2d). It was found that when the concentration of PMS was 1.6–4.0 mM, CTD in the system could be completely decomposed within 2 h, and 1.6 mM PMS was used in the subsequent study. With a view to investigate the interference of system environment on BC@Fe_3S_4 + PMS + CTD, the pH value and temperature of the system were adjusted and controlled. As shown in Fig. 2e and Fig. 2f, it was found that the degradation of CTD by BC@Fe_3S_4 + PMS proceeded more smoothly in the acidic system, while the degradation reaction was inhibited in the alkaline condition. The degradation effect of BC@Fe_3S_4 + PMS + CTD system was excellent in the temperature range of 288.15–308.15 K. From the above experimental results, it can be found that BC@Fe_3S_4 + PMS system had a strong anti-interference ability, could degrade the residual CTD in soil in a wide range, and could also be converted into nitrogen fertilizer (NH_4^+-N) that can be absorbed by crops.

In order to further clarify the mineralization ability of BC@Fe_3S_4 + PMS system to CTD, the TOC removal

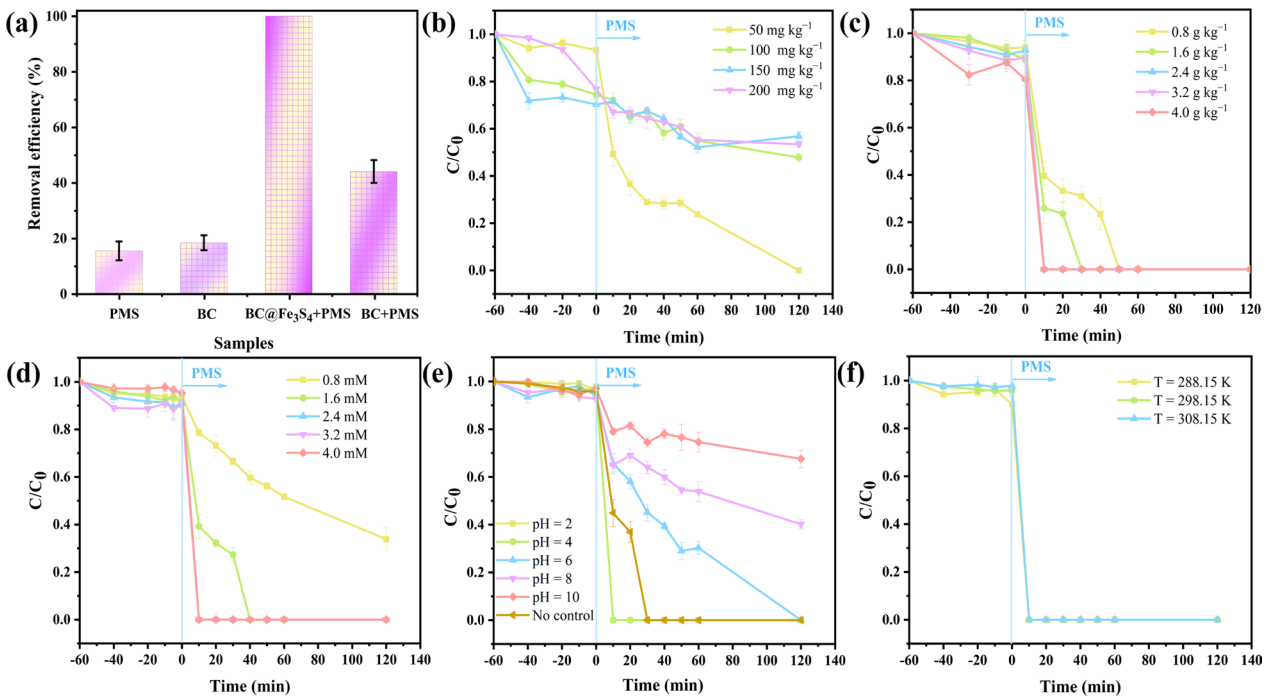

Fig. 2 CTD degradation ability of catalyst under different conditions. **a** catalyst, **b** CTD-concentrations, **c** BC@Fe_3S_4 dosage, **d** PMS concentrations, **e** pH, **f** Temperature. Test environment: all the above experiments were carried out in CTD-contaminates the soil. The reaction equilibrium time is 3 h (adsorption stage is 1 h, degradation stage is 2 h). CTD-contaminates soil = 5.00 g, aqueous volume = 50 mL, catalyst dosage = 0.8 g kg^{-1}, [CTD] = 50 mg kg^{-1}, [PMS] = 1.6 mM, pH = No adjustment, T = 298.15 K

efficiency in BC@Fe_3S_4 + PMS + CTD system was tested. As shown in Fig.S5, the TOC removal efficiency of BC@Fe_3S_4 + PMS system for CTD of 20 mg L^{-1} was as high as 42.79%. This result indicates that the BC@Fe_3S_4 + PMS system exhibited excellent catalytic degradation ability and could effectively decompose and mineralize CTD, even at high concentrations. In order to investigate the stability of BC@Fe_3S_4 + PMS in the actual soil environment restoration process, this study conducted five cyclic degradation experiments on BC@Fe_3S_4 + PMS + CTD system, and tested the degradation ability of BC@Fe_3S_4 + PMS system under low soil and water ratio. As shown in Fig.S6-Fig.S8, the CTD removal efficiency could reach 100% when used for the first time, and the degradation efficiency decreased with the increase of the number of uses. However, after repeated use for five times, the CTD degradation efficiency could remain above 53.49%. This may be due to the loss of Fe_3S_4 during the CTD degradation cycle. At the same time, SEM and EDS tests were conducted on BC@Fe_3S_4 before and after degradation for five times, and the results are shown in Fig. S7. The images showed that the surface structure of BC@Fe_3S_4 remained intact after multiple uses. Finally, in order to explore the potential of BC@Fe_3S_4 + PMS to reduce CTD in the actual soil and water ratio, four degradation experiments with soil and water ratio (1: 1, 1: 2, 1: 5, 1: 10) were set up in this study to more accurately simulate the catalytic activity and actual repair ability of BC@Fe_3S_4 in the actual soil environment with low water content. The degradation ability of BC@Fe_3S_4 + PMS on CTD under different soil and water ratios is shown in Fig. S8. It can be found that the degradation ability of BC@Fe_3S_4 + PMS system on CTD would decrease in soil with low water content, but in the case of low water content where water: soil = 1: 1, the removal efficiency of CTD could be as high as 62.39%. This may be due to the influence of mass transfer between several reactants in the low water content system. Overall, the above results confirmed that the BC@Fe_3S_4 + PMS system had good cycle stability and excellent mineralization ability for CTD. It was further confirmed that BC@Fe_3S_4 + PMS system had great application potential in the remediation of soil organic insecticide.

3.2.3 Effects of CTD and BC@Fe_3S_4 + PMS + CTD systems on lettuce

To investigate the pesticide residues in lettuce and the remediation effect of BC@Fe_3S_4 on contaminated soil, this study set up soil samples contaminated with CTD at various concentrations: 0 mg kg^{-1} (Control group, represented as Control Check (CK)), 0.5 mg kg^{-1}, 5 mg kg^{-1}, 10 mg kg^{-1}, 15 mg kg^{-1}, 20 mg kg^{-1}. Additionally, we established systems for CTD and BC@Fe_3S_4 + CTD + PMS treatment to evaluate their performance. On the 30th day after planting, the camera was used to capture the high-definition picture of lettuce Fig.S9. WSEENLA-S plant root scanner was used to analyze raw lettuce biomass such as fresh weight and dry weight, root volume, root length, leaf area and other basic agronomic parameters to clarify the effects of different concentrations of CTD stress on lettuce growth and CTD residue in lettuce (Fig. S10). It was further verified that BC@Fe_3S_4 + CTD + PMS treatment group could reduce the residue of CTD in lettuce and confirmed that the nutrient conversion products in the system could promote the growth of lettuce.

At the same time, 0.5 g lettuce was randomly sampled for different treatments of each system, and extracted and detected according to the method reported in the literature (Hirano et al. 2019; Tooker and Pearsons 2021; Zhang et al. 2019). See Text S5 for detailed operation methods, and the results are shown in Fig. 3a, on the whole, when the CTD concentration in soil was within the range of 0–20 mg kg^{-1}, the CTD content in lettuce increased with the increase of the initial concentration, while no CTD was detected after the BC@Fe_3S_4 + PMS system was added. The specific situation is as follows: for the CTD stress group, 0.0384 mg kg^{-1} pesticide residues were detected in lettuce when the residual concentration of CTD in soil was 0.5 mg kg^{-1}. When the residual concentration of CTD in soil was more than 0.5 mg kg^{-1}, that is, 5 mg kg^{-1}, 10 mg kg^{-1} and 15 mg kg^{-1}, pesticide residues of 1.2605 mg kg^{-1}, 1.7569 mg kg^{-1} and 1.8204 mg kg^{-1} were detected in lettuce, respectively. However, the maximum pesticide residue 2.9228 mg kg^{-1} was detected in lettuce when the residual concentration of CTD in soil was the highest (20 mg kg^{-1}). Thus, it can be seen that the residual amount of CTD in lettuce increased with the initial CTD concentration in the soil. For the BC@Fe_3S_4 + CTD + PMS system, no CTD residue was detected in the lettuce under each treatment, indicating that CTD in the soil had been completely degraded. It is confirmed that BC@Fe_3S_4 + PMS could remove CTD residue in soil and avoid the possibility of pesticide entering human body.

The effects of different concentrations of CTD stress and BC@Fe_3S_4 + PMS + CTD detoxification/nutrient conversion on lettuce growth and dry matter accumulation were determined. Detailed test methods for fresh and dry weight of lettuce are in Text S11. As shown in Fig. 3b and Fig. 3c, it can be found that when CTD concentration in soil was 0 mg kg^{-1}, the fresh weight and dry weight of each lettuce plant in healthy soil and healthy soil + BC@Fe_3S_4 + PMS system were 0.2616 g and 0.2433 g, respectively, and 15.9333 mg and 16.4667 mg, respectively. There was no significant change in fresh weight and dry weight of lettuce, indicating that BC@

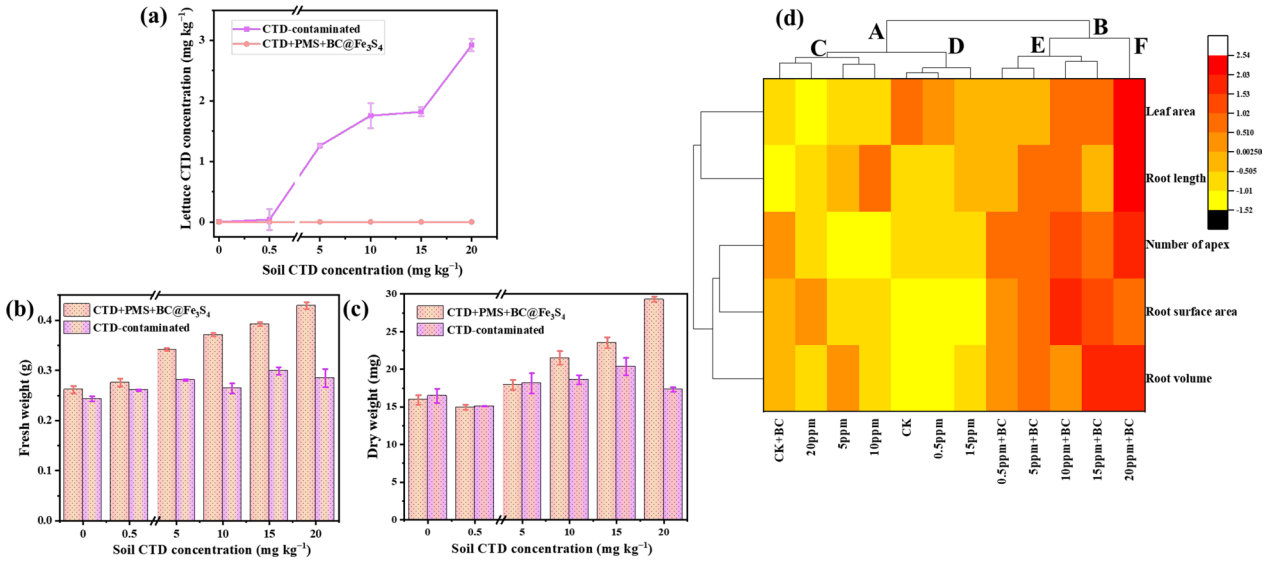

Fig. 3 Results of samples taken on day 30th after lettuce planting in the control group (CTD) and the experimental group (CTD + BC@Fe_3S_4 + PMS). **a** CTD residual concentration in lettuce plants under different treatments, **b** lettuce seedling biomass (fresh weight) under different treatments, **c** dry matter accumulation of lettuce plants under different treatments, **d** cluster heat map analysis of various agronomic traits of lettuce plants under different treatments, yellow and red in the matrix box show strong negative correlation and positive correlation. Due to space constraints when drawing heat maps, some abbreviations are used in Fig. 3, which are explained below. BC in Fig. 3 refers to the BC@Fe_3S_4 + PMS processing group; 0.5, 5, 10, 15, 20 ppm refers to 0.5, 5, 10, 15, 20 mg kg^{-1} CTD-contaminated soil; CK refers to fresh soil that has not been contaminated by CTD.

Fe_3S_4 + PMS itself could not promote the growth of lettuce. As shown in Fig. 3, compared with lettuce cultured in healthy soil, fresh weight and dry weight of lettuce under different CTD concentrations (0.5–20 mg kg^{-1}) not only did not decrease significantly, but also increased slightly. The possible reason is that CTD, as a touch, gastric toxicity and endogenic insecticide, has less impact on the growth of plants. However, it will enter the food chain after absorption by crops, and eventually endanger human health. At the same time, active substances in the soil can cause a small amount of CTD to be broken down into nutrients, promoting the growth of lettuce. Soil containing different CTD-concentrations (0–20 mg kg^{-1}) were treated with BC@Fe_3S_4 + PMS system. It was found that the fresh weight and dry weight of lettuce in BC@Fe_3S_4 + PMS + CTD treatment group increased with the increase of initial CTD concentration in soil. The possible reason is that BC@Fe_3S_4 + PMS system could convert residual CTD in soil into nutrients that can be absorbed by lettuce. The higher the concentration of residual CTD, the more NH_4^+-N will be converted into, and the more vigorous the growth of lettuce.

In order to better understand the reasons for changes in fresh and dry weight of lettuce, Cluster heatmap was used to conduct correlation analysis on basic agronomic parameters such as root volume, root length, leaf area and number of root tips of lettuce. As shown in Fig. 3d, it can be seen that the 12 treatment groups were orderly divided into A and B. Class A was composed of 7 treatments, including healthy soil, healthy soil + BC@Fe_3S_4 + PMS, and different CTD stress (0.5–20 mg kg^{-1}). Five treatment groups of the BC@Fe_3S_4 + PMS + CTD system (in the initial CTD concentration range of 0.5–20 mg kg^{-1}) were classified as Class B. This further proves that BC@Fe_3S_4 + PMS could convert CTD into nutrients that can be absorbed by crops, and promote the growth of root length and leaf area, which is also consistent with the results of the changes of fresh weight and dry weight.

In summary, lettuce seedlings could absorb and accumulate CTD in the body, and with the increase of the concentration of CTD, the residual amount in lettuce would also increase. When the BC@Fe_3S_4 + PMS was added to soil contaminated with CTD, it not only successfully degraded CTD, but also broke it down into NH_4^+-N, providing part of the fertilizer source for lettuce and promoting the growth of lettuce. At the same time, the soil organic pollution was repaired and the farmland production environment was improved. These results verified the importance of removing CTD pollution and the feasibility of BC@Fe_3S_4 in soil remediation, and also provided a new idea for removing soil organic pollution.

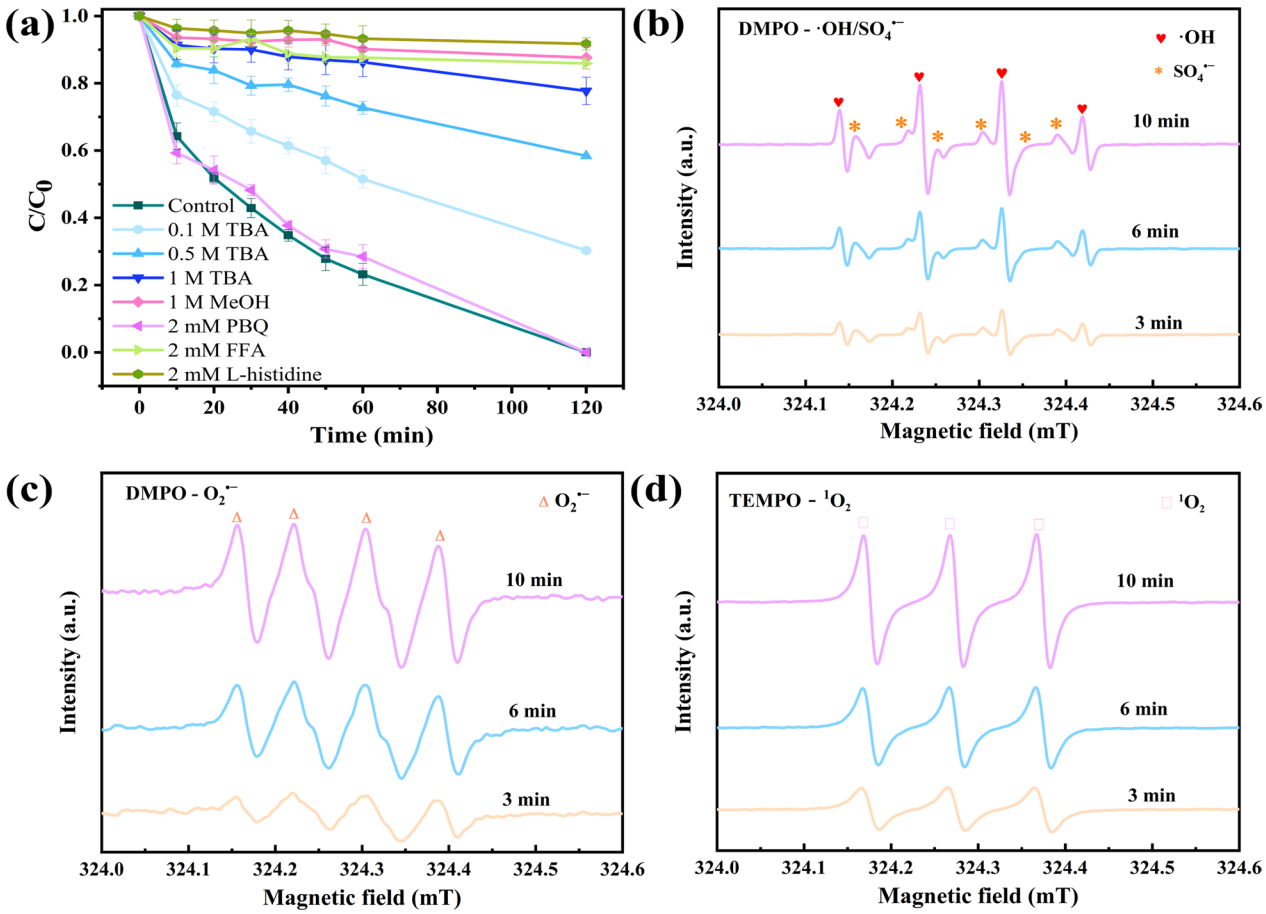

Fig. 4 **a** Effect of free radical quencher on the degradation of CTD. To identify the dominant ROS, TBA (0.1, 0.5, 1 M), MeOH (1 M), PBQ (2 mM), FFA (2 mM)), L-histidine (2 mM) were employed as radical scavengers. ESR spectra of different ROS: **b** $SO_4^{\bullet-}$ and •OH, **c** $O_2^{\bullet-}$, (d)$^1O_2$. The above experiments were carried out in a mixture of water and soil. CTD-contaminates soil = 5.00 g, aqueous volume = 50 mL, catalyst dosage = 0.8 g kg^{-1}, [CTD] = 50 mg kg^{-1}, [PMS] = 1.6 mM, pH = No adjustment, T = 298.15 K

3.3 Mechanism of catalysis and nutrition conversion in BC@Fe_3S_4 + PMS + CTD system

3.3.1 Production and mechanism of active oxygen species (ROS)

Five quenchers (methanol, L-histidine, furfuryl alcohol, p-benzoquinone and tert-butanol) were selected to identify ROS involved in CTD degradation (The second-order reaction rates between the five quenchers and ROS are shown in Table S4). As shown in Fig. 4a, after adding 1.0 M MeOH to BC@Fe_3S_4 + PMS + CTD system, the degradation efficiency of CTD was significantly reduced to 12.40%. Due to the high second-order reaction rate of MeOH to •OH and $SO_4^{\bullet-}$, the above results indicate that •OH and $SO_4^{\bullet-}$ play an important role in the degradation of CTD (Guo et al. 2022; Yang et al. 2023; Yuan et al. 2021). In order to further determine which ROS occupied the dominant position in the BC@Fe_3S_4 + PMS + CTD system, tert-butanol with stronger binding ability to •OH was selected (Huang et al. 2023; Qi et al. 2020; Xu et al. 2024), and 0.10M, 0.5M and 1M TBA were added, respectively. The results showed that CTD degradation efficiency decreased from 69.70% to 22.27% as TBA concentration increased from 0.10 M to 1 M. The research results of Huang et al. also showed a similar trend of change and concluded that •OH was the dominant free radical (Huang et al. 2023). It can be reasonably inferred from the above results that •OH was dominant in the BC@Fe_3S_4 + PMS + CTD system. p-BQ quenching $O_2^{\bullet-}$ and FFA/ L-histidine quenching of $^1O_2$ were used to determine the contribution of $O_2^{\bullet-}$ and $^1O_2$ to the degradation of CTD in BC@Fe_3S_4 + PMS + CTD system. It can be found that in the presence of p-BQ, CTD degraded normally. The CTD removal rate of BC@Fe_3S_4 + PMS + CTD system in the presence of FFA decreased to 14.11%. When L-histidine was added, the degradation efficiency of CTD decreased to 8.28%, indicating that $^1O_2$ was an important reason for the degradation of CTD. The above experimental results prove that

•OH, $^1O_2$ and $SO_4^{\bullet-}$ were the most important ROS in BC@Fe_3S_4 + PMS + CTD system.

With a view to more intuitively understand the species of ROS present in BC@Fe_3S_4 + PMS + CTD system, DMPO and TEMPO were used as spin capture agents to conduct ESR tests on BC@Fe_3S_4 + PMS + CTD system, and the results are shown in Fig. 4b-d. It can be found that four ROS, •OH, $^1O_2$, $SO_4^{\bullet-}$ and $O_2^{\bullet-}$, all appeared in BC@Fe_3S_4 + PMS + CTD system, and their signal peaks increased with time. It was confirmed that BC@Fe_3S_4 + PMS + CTD system produced a variety of ROS such as •OH, $^1O_2$, $SO_4^{\bullet-}$ and $O_2^{\bullet-}$, which provided conditions for the degradation and nutrient conversion of CTD.

3.3.2 *Analysis of catalytic activity and mechanism of BC@Fe_3S_4*

In order to clarify the mechanism of BC@Fe_3S_4 activated PMS degradation and conversion of CTD. XPS was used to compare the valence states of C, O, S, and Fe on BC@Fe_3S_4 surface before and after the reaction, as shown in Fig. 5 and Fig. S11. It can be seen from Fig. 5a and d that the surface of BC@Fe_3S_4 before and after catalysis was mainly composed of C1s, O1s, Fe2p and S2p. It can be seen from the total spectrum of XPS that the changes were not drastic, which may be one of the reasons why the material can maintain stability. Then, Fe2p and S2p were peak fitted, and the fitting results are shown in Fig. 5b, c, and e, f. Fe^{2+}, Fe^{3+} and satellite peaks can be analyzed in $Fe2p_{3/2}$ and $Fe2p_{1/2}$, indicating that the iron on the surface of BC@Fe_3S_4 mainly existed in the form of Fe^{2+} and Fe^{3+} (Li et al. 2024). By comparing the valence changes of BC@Fe_3S_4 iron before and after the catalytic reaction, it can be found that the peak area percentage of Fe^{2+} before the BC@Fe_3S_4 reaction was as high as 54.60%, but after the degradation reaction, the proportion of Fe^{2+} decreased to 14.47%, and the proportion of Fe^{3+} rapidly increased to 85.53%. It was confirmed that Fe^{2+} participated in the catalytic degradation of BC@Fe_3S_4 + PMS + CTD system by giving electrons. At the same time, the existing S2p in the system was analyzed. As can be seen from Fig. 5c and f, there were abundant forms of S2p in BC@Fe_3S_4, and four peaks could be obtained by sub-peak fitting. If the binding energy is arranged from low to high, the four peaks belong to S^{2-}, S_n^{2-}, SO_4^{2-} ($S2p_{3/2}$) and SO_4^{2-} ($S2p_{1/2}$), respectively (Ding et al. 2023; Gao et al. 2022a, 2022b; Hong et al., 2021). This confirms that BC@Fe_3S_4 contained multiple forms of sulfur with the potential to provide electrons for the Fe^{3+}/Fe^{2+} cycle and to activate PMS. Figure 5f also shows the XPS spectrum of S2p in BC@Fe_3S_4 after the degradation reaction. It can be found that after the degradation reaction, the content of S^{2-} decreased from 52.19% to 48.77%, while the content of S_n^{2-} increased from

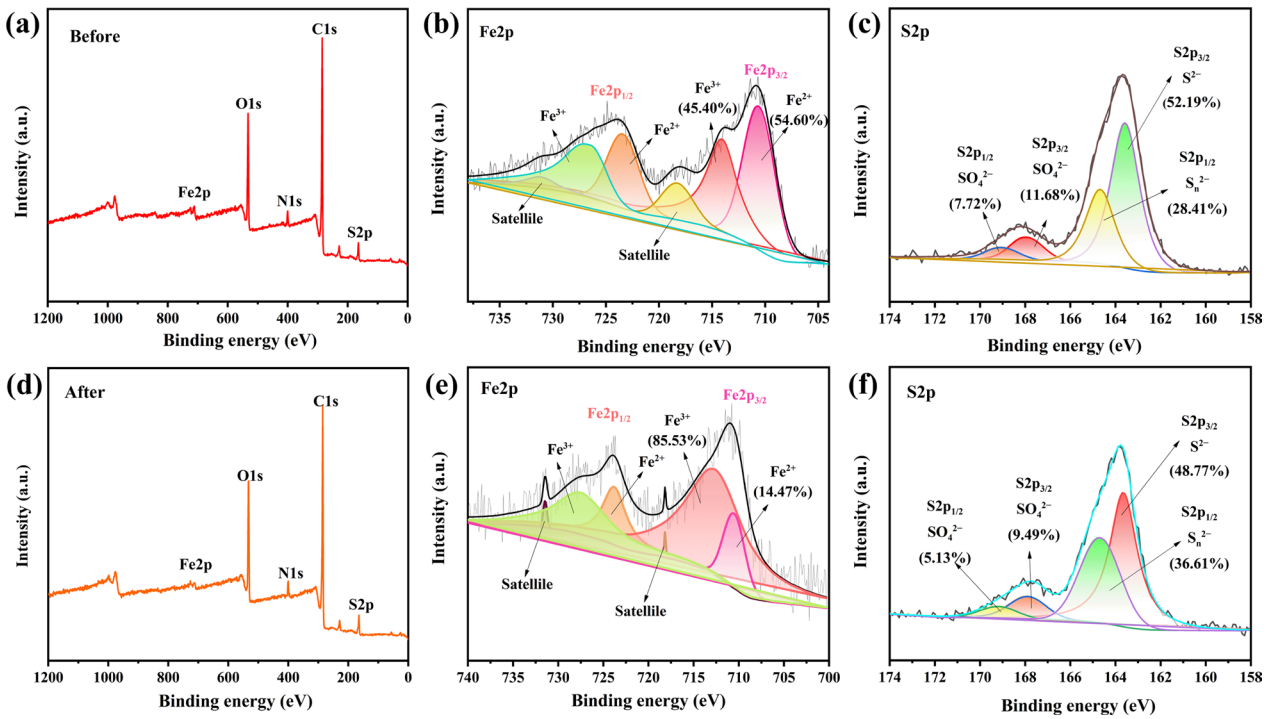

Fig. 5 **a**–**c** is the XPS test result of BC@Fe_3S_4, and **d**–**f** is the total spectrum, Fe2p and S2p of XPS after the reaction of BC@Fe_3S_4 + CTD + PMS system

28.41% to 36.61%. These results suggest that S^{2-} may be involved in Fe^{3+}/Fe^{2+} cycling and catalytic degradation in BC@Fe_3S_4 + PMS + CTD system as an electron donor. Subsequently, O1s and C1s in BC@Fe_3S_4 were peak fitted, and the results are shown in Fig.S11. It can be found that BC@Fe_3S_4 was rich in oxygen-containing functional groups, which is also consistent with the FT-IR analysis results in Fig.S1d, indicating that BC@Fe_3S_4 had high hydrophilicity, which is conducive to the degradation reaction in BC@Fe_3S_4 + PMS + CTD system. These results indicate that BC@Fe_3S_4 was a composite material containing polyvalent iron and sulfur and modified with rich functional groups. The excellent degradation/transformation ability of BC@Fe_3S_4 + PMS + CTD system may be attributed to the consumption of Fe^{2+} and reduction of Fe^{3+} by S^{2-}.

The specific reactions that may be involved in the BC@Fe3S4 + PMS + CTD system are shown in eqs.1–13. Equations 1–3 describe the process by which Fe^{2+} catalyzes the PMS to produce $SO_4^{\bullet-}$ and •OH in the BC@Fe_3S_4 + PMS + CTD system, while the Fe^{2+} on the BC@Fe_3S_4 surface is oxidized to Fe^{3+} (Gao et al. 2022b). Equations 4–10 describe the process of generation of ROS such as •OH, $O_2^{\bullet-}$ and $^1O_2$ (Ding et al. 2023; Hong et al. 2021). First, $SO_4^{\bullet-}$reacts with H_2O to form •OH (Eq. 4), then reacts with HSO_5^- with H_2O to form H_2O_2 (Eq. 5), and then reacts with •OH and H_2O_2 to form HO_2• (Eq. 6). HO_2• cannot exist stably and is easy to decompose to produce $O_2^{\bullet-}$ (Eq. 7). At the same time, free radicals such as HO_2•, $O_2^{\bullet-}$ and •OH may react to form $^1O_2$ (eqs.8–10). Equations 11–12 describe the REDOX reaction of sulfur (Gao et al. 2022a, 2022b). In Eq. 11, S^{2-} is oxidized to S_n^{2-} by Fe^{3+}, while Fe^{3+} is reduced to Fe^{2+}. In Eq. 12, S_n^{2-} is further oxidized to SO_4^{2-}, while Fe^{3+} is again reduced to Fe^{2+}. Equation 13 describes the process in which CTD was converted into various intermediates under the action of ROS such as •OH, $^1O_2$, $SO_4^{\bullet-}$ and finally degraded into NH_4^+-N, CO_2 and H_2O. This reaction pathway indicates the degradation mechanism of CTD in the BC@Fe_3S_4 catalytic system.

$$Fe^{2+} + HSO_5^- \rightarrow Fe^{3+} + SO_4^{\cdot-} + OH^- \quad (1)$$

$$Fe^{2+} + HSO_5^- \rightarrow Fe^{3+} + SO_4^{2-} + \cdot OH \quad (2)$$

$$HSO_5^- + e^- \rightarrow SO_4^{2-} + \cdot OH \quad (3)$$

$$SO_4^{\cdot-} + H_2O \rightarrow \cdot OH + SO_4^{2-} + H^+ \quad (4)$$

$$HSO_5^- + H_2O \rightarrow H_2O_2 + HSO_4^- \quad (5)$$

$$\cdot OH + H_2O_2 \rightarrow HO_2^- + HO_2\cdot \quad (6)$$

$$HO_2\cdot \rightarrow O_2^{\cdot-} + H^+ \quad (7)$$

$$HO_2\cdot + O_2^{\cdot-} \rightarrow {}^1O_2 + HO_2^- \quad (8)$$

$$O_2^{\cdot-} + \cdot OH \rightarrow {}^1O_2 + OH^- \quad (9)$$

$$2O_2^{\cdot-} + H_2O \rightarrow {}^1O_2 + 2OH^- + H_2O_2 \quad (10)$$

$$S^{2-} + Fe^{3+} \rightarrow Fe^{2+} + S_n^{2-} \quad (11)$$

$$S_n^{2-} + Fe^{3+} \rightarrow Fe^{2+} + SO_4^{2-} \quad (12)$$

$$CTD + \cdot OH + {}^1O_2 + SO_4^{\cdot-} \rightarrow CTD_{intermediates} \rightarrow NH_4^+ - N + CO_2 + H_2O \quad (13)$$

3.3.3 Nutrient transformation, degradation pathway and toxicity evaluation of intermediates of CTD

The degradation and nutritive intermediates in BC@Fe_3S_4 + CTD + PMS system and their transformation mechanism were determined. Previous studies have shown that ROS such as •OH, $^1O_2$, and $SO_4^{\bullet-}$, which are produced after the catalytic decomposition of PMS, have a strong attack ability, and these ROS dominate the degradation of NEOs (Elumalai et al. 2022; Lee et al. 2022; Nguyen Tien et al. 2023; Sales-Alba et al. 2023). The CTD degradation intermediates in BC@Fe_3S_4 + CTD + PMS system were tested and analyzed. The results are shown in Fig.S12, Fig. 6 and Table S5. Fig.S12 shows the LC–MS/MS of CTD and the main intermediates in the degradation process of BC@Fe_3S_4 + CTD + PMS, and predicts the CTD degradation path as shown in Fig. 6. CTD degradation mechanisms may include hydroxylation, carboxylation, carbonylation, hydrolysis and dechlorination. Figure 6 illustrates three possible transformation and degradation pathways (Liu et al. 2021; Zhang et al. 2020).

First, pathway 1 is the mechanism that does not replace Cl, and hydroxylation is the main mechanism of degradation system. After hydrolysis of the C − N bond and C − C bond at the end of the branch chain, the original chemical group can be replaced by •OH and $^1O_2$ to form small molecules (P1, ($C_5H_7ClN_2O_4S$)) (Duan et al. 2020; Wang et al. 2019). The H connected to the C at the middle of the branch chain is also easily destroyed by •OH and $^1O_2$, such as decomposition into (P2 ($C_6H_9ClN_4S$), P3 ($C_3H_3NO_2S$)). The carbonylation and carboxylation

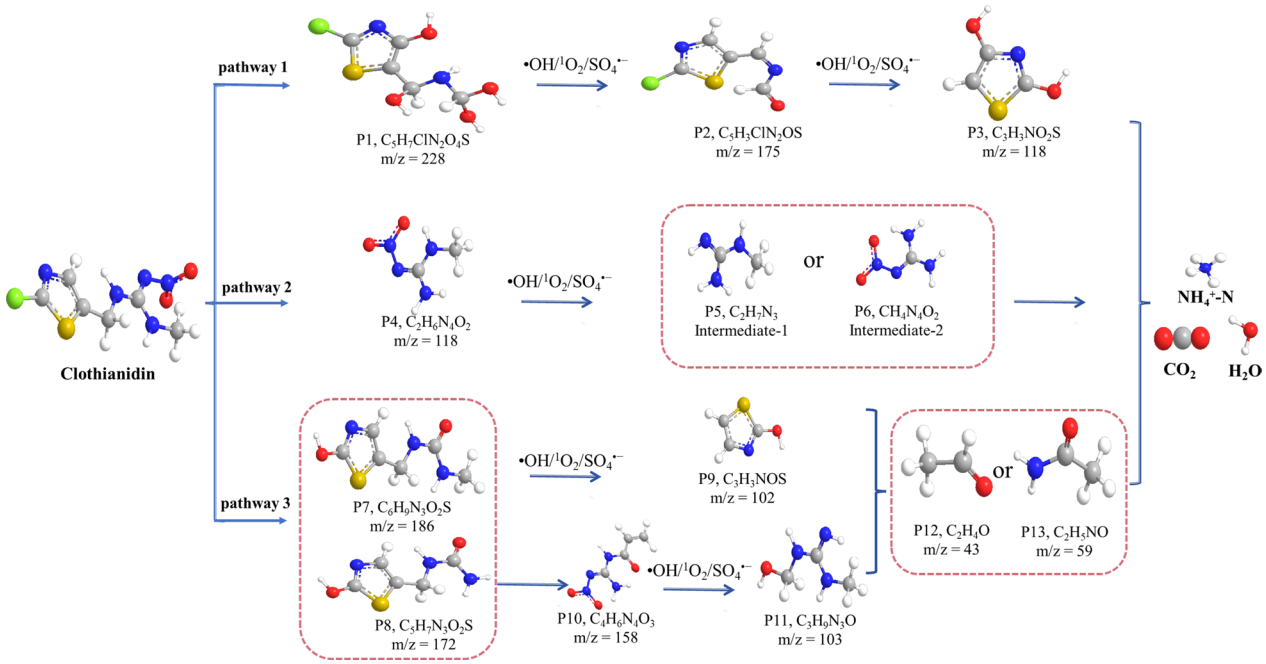

Fig. 6 Possible transformation pathways of CTD in nutritive and degradation systems

of the C=N bond in the oxidation of CTD are based on the hydroxylation of the chemical groups on the H and C atoms, indicating that •OH and $^1O_2$ are still the main oxidizing free radicals for the carboxylation of the system (Abdel-Ghany et al. 2016). Pathway 2, which is caused by the radical attacking the C–N bond on the parent ion, forming the compound (P4 ($C_2H_6N_4O_2$), which is further cleaved to intermediate-1 and intermediate-2 by the •OH, $^1O_2$, and $SO_4^{\bullet-}$. Due to the C–N bond dissociation, P5 ($C_2H_7N_3$) and P6 ($CH_4N_4O_2$) are further cleaved by •OH, $^1O_2$, and $SO_4^{\bullet-}$ to form CO_2, H_2O, NH_4^+-N, etc. (Žabar et al. 2012; Zhang et al. 2020). The pathway 3 is dechlorination. CTD is first transformed into P7 ($C_6H_9N_3O_2S$) and P8 ($C_5H_7N_3O_2S$) by dechlorination, per-carboxylation and chain breaking. It's worth noting that these two molecules can form in different ways. First, P7 ($C_6H_9N_3O_2S$) molecules are further attacked by hydroxyl radical C–C bond fracture into P9 (C_3H_3NOS), and then further oxidized into small molecules. Secondly, P8 ($C_5H_7N_3O_2S$) molecules are ketozed or hydroxyl to form P10 ($C_4H_6N_4O_3$) and P11 ($C_3H_9N_3O$) molecules under the joint action of •OH, $^1O_2$, and $SO_4^{\bullet-}$ (Duan et al. 2020). Finally, CTD is further decomposed into P12 (C_2H_4O) and P13 (C_2H_5NO) small molecular weight intermediates, and CTD is finally decomposed into CO_2, H_2O and NH_4^+-N through these different bond-breaking pathways.

The above research results show that the three main degradation pathways involved in BC@Fe_3S_4+CTD+PMS system were hydroxylation, hydrolysis and dechlorination, and finally the decomposition of CTD into H_2O, CO_2, and NH_4^+-N. In this study, T.E.S.T-QSAR (Text S9 includes software and specific application methods for toxicity analysis of degradation intermediates) was used to assess the toxicity changes of intermediates involved in the degradation/nutrient conversion process of CTD on Fathead minnow and T.pyriformis (Ding et al. 2023; Wen et al. 2024). As can be seen from Fig. 7 and Table S5, the toxicity of intermediates produced by the three main degradation pathways to Fathead minnow and T.pyriformis basically showed a decreasing trend. Of the three major CTD degradation pathways of the BC@Fe_3S_4+CTD+PMS system, the toxicity of pathway 1 decreased slightly, which may be related to the presence of chloride ions in the intermediate. The toxicity of intermediates in pathway 2 and pathway 3 was significantly reduced, possibly due to dechlorination and ring-opening reactions. In summary, during the decomposition of CTD into H_2O, CO_2, and NH_4^+-N in BC@Fe_3S_4+CTD+PMS system, the toxicity of the intermediates to organisms also decreased. This further confirms the practical application potential of BC@Fe_3S_4+PMS.

3.4 Research prospects

Although this study has made some achievements in the nutrient conversion/degradation of soil organic insecticide (clothianidin), biochar composite catalyst synthesis, biochar composite activated persulfate removal

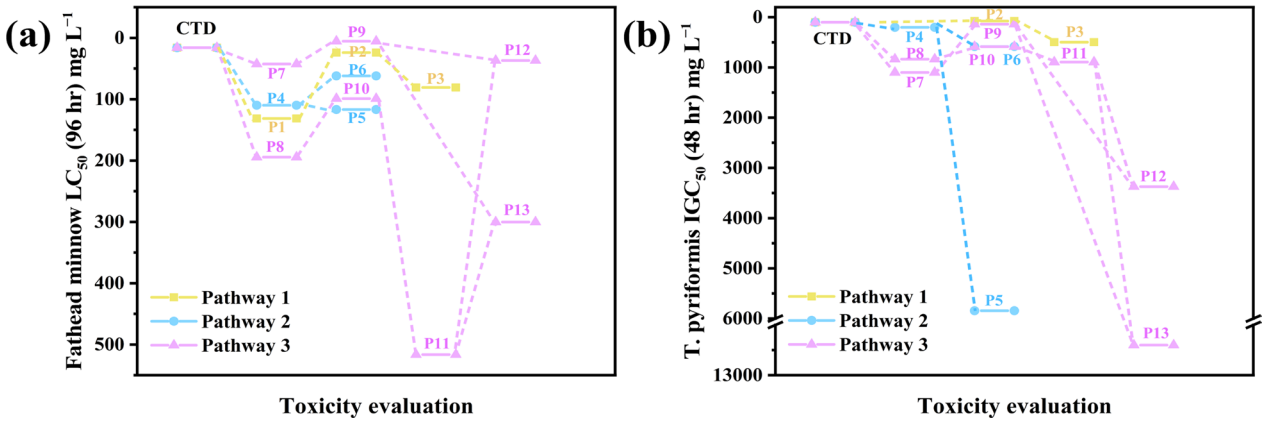

Fig. 7 T.E.S.T-QSAR evaluated the toxicity of CTD and its intermediates to Fathead minnow (**a**) and T.pyriformis (**b**)

mechanism of organic insecticide, there are still some limitations. For example, due to time, technology, and resource constraints, we regret not being able to explore the following areas in depth:

1. In the experiment of BC@Fe_3S_4 catalyzing PMS to degradation of CTD, there is a correlation between the amount of catalyst, the amount of oxidant, the concentration of pollutants and other factors. It is limited to select the best reaction conditions through single factor experiment. Subsequent researchers can use methods such as multi-factor orthogonal experiment in this part to more comprehensively reveal the interaction between various factors and obtain more accurate results.
2. In this study, the generation mechanism and main active species of ROS in BC@Fe_3S_4 + PMS + CTD system were investigated through ESR and quenching experiments. These experimental results provide an important basis for understanding the role of ROS in the degradation and nutrient conversion process of the soil organic insecticide CTD. However, since the focus of this study is not on the specific contribution efficiency of each ROS in the CTD degradation process, the precise calculation of the steady-state concentration of free radicals has not been further carried out in this study. As a result, the steady-state concentration of ROS produced in BC@Fe_3S_4 + PMS + CTD system and the specific contribution efficiency of each ROS in the CTD degradation process are still unclear. In future studies, subsequent researchers can accurately calculate the steady-state concentration of ROS in the system by establishing a suitable kinetic model and combining experiments to determine the reaction rate constants of ROS and probe chemicals. This will help to clarify the specific contribution mechanism of various ROS in the degradation process of organic pollutants.
3. Through consulting a large number of literatures in related fields, it is found that ferrous sulfide composites have been widely used in batteries and supercapacitors in the past few decades due to their excellent electrochemical properties (Guo et al. 2016; Yang et al. 2017; Yu et al. 2018). In recent years, researchers have found that ferrous sulfide/biochar composites have excellent catalytic ability and have been applied to activate persulfate to remove environmental organic pollutants (Hong et al. 2021; Ma et al. 2023). In terms of degradation, a large number of existing catalyst + PMS + organic pollutant degradation systems are concentrated in theoretical and mechanism studies. The main experiments are done in distilled water/ultra-pure water. A large number of researchers believe that remediation of organic pollutants in actual wastewater and soil is particularly important (Chen et al. 2018; Diao et al. 2021). But there is still a long way to go from distilled/ultra-pure water to actual environmental remediation. At the same time, a small amount of literature has proposed that organic pollutants may generate small molecular acids and nutrients during the degradation process (Chen et al. 2019; Wen et al. 2022). In this study, BC@Fe_3S_4 composite was synthesized by a one-step method. BC@Fe_3S_4 can convert CTD into NH_4^+-N by stimulating PMS in soil system. The mechanism involved was analyzed. The effects of CTD stress and BC@Fe_3S_4 + PMS treatment group on CTD residue and dry matter accumulation in lettuce were also observed. This work is conducive to promoting the research progress in the field of biochar composites remediation of soil organic pollutants. In this study, the greenhouse pot experiment of lettuce was

used to investigate the excellent properties of BC@Fe_3S_4+PMS system. Although this can prove the detoxification ability of BC@Fe_3S_4+PMS system to a certain extent, it is not conducive to the study of the long-term effectiveness, environmental safety and practical operability of BC@Fe_3S_4+PMS. In view of the above defects, subsequent researchers may consider adding post-crop planting experiments to the pot experiment to ensure its long-term sustainability. Where available, further use of long-term field trials is recommended to assess the practicability, environmental safety and durability of biochar.

In addition, future research can also consider the synthesis of non-metallic modified biochar, physical modified biochar and other materials to repair soil organic pollutants, which is conducive to reducing the risk of catalytic materials to the environment. Further improve the shortcomings of research on biochar removal/conversion of soil organic pollutants and promotion of crop growth. In addition, combining biochar materials with professional fields of agriculture, chemistry, environment and other disciplines may find new research perspectives and application value. We look forward to future studies addressing these unanswered questions and advancing the continued development of biochar+AOPs systems in the field of agro-environmental remediation.

4 Conclusion

In summary, a biochar modified with Fe_3S_4 and oxygen-containing functional groups (BC@Fe_3S_4) was synthesized by one-step hydrothermal method in this paper, which had excellent catalytic effect and electron transfer ability, and could degrade and nutritionally transform residual CTD in soil. In addition, the ability of BC@Fe_3S_4+PMS system to convert soil CTD to NH_4^+-N and its effects on dry matter accumulation and CTD residue in lettuce were investigated. The results showed that the CTD degradation efficiency of BC@Fe_3S_4+PMS could reach 100% when the initial concentration of CTD in soil and water mixture was 5 mg L^{-1}. When the initial concentration of CTD in soil and water mixture was 20 mg L^{-1}, NH_4^+-N in the system treated by BC@Fe_3S_4+PMS could reach 3.029 mg L^{-1}. The results showed that when the concentration of CTD in potting soil was 20 mg kg^{-1}, the dry weight of lettuce was 17.3 mg/ plant, and the residual concentration of CTD in lettuce was as high as 2.9228 mg kg^{-1}. After BC@Fe_3S_4+PMS treatment, the dry weight of the lettuce was 29.3 mg/ plant, and no CTD residue was detected. BC@Fe_3S_4+PMS+CTD system mainly catalyzed PMS to produce ROS such as •OH, $^1O_2$ and $SO_4^{\bullet-}$ through biochar and surface-active ingredients (Fe and S, etc.), thereby efficiently degrading and converting CTD. In this study, a biochar composite catalyst (BC@Fe_3S_4) with simple preparation method and high catalytic activity was introduced. BC@Fe_3S_4 could degrade CTD in soil environment and convert it into NH_4^+-N, which not only removed CTD in contaminated soil and lettuce, but also promoted dry matter accumulation in lettuce. This study clarified the mechanism of conversion of organic insecticide CTD to NH_4^+-N, and provided a feasible strategy for biochar remediation of organic insecticides in contaminated soil. We have reason to believe that this study has certain reference value for practical applications in the fields of "biochar remediation of agricultural organic contaminated soil" or "conversion of organic pollutants into nutrients" in the future.

Supplementary Information

The online version contains supplementary material available at https://doi.org/10.1007/s42773-025-00465-z.

Supplementary Material 1.

Acknowledgements
The authors sincerely acknowledge the anonymous reviewers for their insights and comments to further improve the quality of the manuscript.

Author contributions
All authors contributed to the study conception and design. Materials preparation and degradation experimental data were collected by Dong He, and degradation mechanism was analyzed by Yujiao Wen. All experiments were supervised by Yujiao Wen and completed by Dong He. The first draft of the manuscript was written by Yujiao Wen and all authors commented on previous versions of the manuscript. Hongmei Liu and Zhonghua Zhou provides guidance on article revision. Nan Zhou: Writing-review, editing and supervision. All authors read and approved the final manuscript.

Funding
The authors would like to show great acknowledgements for the financial support from the Distinguished Youth Foundation of Hunan Province (2022JJ10030), Key R&D projects in Hunan Province (2022NK2044), the Natural Science Foundation of Hunan Province, China (2021JJ40261), and the science and technology innovation Program of Hunan Province (2022WZ1022). This research was funded by "Hunan Provincial Cotton Industry Technology System Cultivation and Seed Breeding Post Expert Program" grant number "XIANGNONGFA (2022) No. 31", "The Hunan Provincial Department of Agriculture and Rural Affairs Project" grant number "XIANG CAI JIAN ZHI (2024) No. 162", and the Furong Plan Province enterprise science and technology innovation and entrepreneurship team support project (Hunan Talent Office [2024] No.08).

Data availability
The datasets used or analyzed during the current study are available from the corresponding author on reasonable request.

Declarations

Competing interests
The authors declare that they have no known competing financial interests or personal relationships that could have appeared to influence the work reported in this paper.

Author details
[1]Hunan Engineering Research Center for Biochar, Hunan Agricultural University, Changsha 410128, China. [2]College of Mechanical and Electrical Engineering, College of Agronomy, College of Chemistry and Material Science,

Hunan Agricultural University, Changsha 410128, China. [3]Hunan Province Linxiang City Huanggai Town Agricultural Comprehensive Service Center, Linxiang 414000, China. [4]Central South University Institute of Environmental Engineering School of Metallurgy and Environment, 932 Lushan South Road, Changsha 410083, People's Republic of China.

Received: 11 September 2024 Revised: 14 April 2025 Accepted: 21 April 2025
Published online: 27 June 2025

References

Abdel-Ghany MF, Hussein LA, El Azab NF, El-Khatib AH, Linscheid MW (2016) Simultaneous determination of eight neonicotinoid insecticide residues and two primary metabolites in cucumbers and soil by liquid chromatography–tandem mass spectrometry coupled with QuEChERS. J Chromatogr B 1031:15–28. https://doi.org/10.1016/j.jchromb.2016.06.020

Alamgholiloo H, Pesyan NN, Mohammadi R, Rostamnia S, Shokouhimehr M (2021) Synergistic advanced oxidation process for the fast degradation of ciprofloxacin antibiotics using a GO/CuMOF-magnetic ternary nanocomposite. J Environ Chem Eng. https://doi.org/10.1016/j.jece.2021.105486

Bandeira FO, Alves PRL, Hennig TB, Brancalione J, Nogueira DJ, Matias WG (2021) Chronic effects of clothianidin to non-target soil invertebrates: Ecological risk assessment using the species sensitivity distribution (SSD) approach. J Hazard Mater. https://doi.org/10.1016/j.jhazmat.2021.126491

Chen L, Hu X, Yang Y, Jiang C, Bian C, Liu C, Zhang M, Cai T (2018) Degradation of atrazine and structurally related s-triazine herbicides in soils by ferrous-activated persulfate: Kinetics, mechanisms and soil-types effects. Chem Eng J 351:523–531. https://doi.org/10.1016/j.cej.2018.06.045

Chen Q, Rao P, Cheng Z, Yan L, Qian S, Song R, Shen G (2019) Novel soil remediation technology for simultaneous organic pollutant catalytic degradation and nitrogen supplementation. Chem Eng J 370:27–36. https://doi.org/10.1016/j.cej.2019.03.179

Chen Y, Gong M, Liang D, Li S, Meng D, He J, Li Y, Kang Z, Li H (2023) Application of urea hydrogen peroxide: Degradation of glyphosate in soil and effect on ammonia nitrogen effectiveness and enzyme activity. J Environ Chem Eng. https://doi.org/10.1016/j.jece.2023.110949

Chowdhury S, Mukhopadhyay S, Bhattacharyya A (2012) Degradation dynamics of the insecticide: clothianidin (Dantop 50 % WDG) in a tea field ecosystem. Bull Environ Contam Toxicol 89(2):340–343. https://doi.org/10.1007/s00128-012-0671-2

Diao Z-H, Zhang W-X, Liang J-Y, Huang S-T, Dong F-X, Yan L, Qian W, Chu W (2021) Removal of herbicide atrazine by a novel biochar based iron composite coupling with peroxymonosulfate process from soil: synergistic effect and mechanism. Chem Eng J. https://doi.org/10.1016/j.cej.2020.127684

Ding Y, Wang X, Fu L, Peng X, Pan C, Mao Q, Wang C, Yan J (2021) Nonradicals induced degradation of organic pollutants by peroxydisulfate (PDS) and peroxymonosulfate (PMS): Recent advances and perspective. Sci Total Environ. https://doi.org/10.1016/j.scitotenv.2020.142794

Ding C, Liu Z, Pan S, Zhao C, Wang Z, Gao B, Li Q (2023) Activation of peroxydisulfate via Fe@sulfur-doped carbon-supported nanocomposite for degradation of norfloxacin: efficiency and mechanism. ChemEng J. https://doi.org/10.1016/j.cej.2023.141729

Duan P, Qi Y, Feng S, Peng X, Wang W, Yue Y, Shang Y, Li Y, Gao B, Xu X (2020) Enhanced degradation of clothianidin in peroxymonosulfate/catalyst system via core-shell FeMn @ N-C and phosphate surrounding. Appl Catal B Environ. https://doi.org/10.1016/j.apcatb.2020.118717

Ebrahimi A, Jafari N, Ebrahimpour K, Karimi M, Rostamnia S, Behnami A, Ghanbari R, Mohammadi A, Rahimi B, Abdolahnejad A (2021) A novel ternary heterogeneous TiO2/BiVO4/NaY-Zeolite nanocomposite for photocatalytic degradation of microcystin-leucine arginine (MC-LR) under visible light. Ecotoxicol Environ Safety. https://doi.org/10.1016/j.ecoenv.2020.111862

Elumalai P, Yi X, Chen Z, Rajasekar A, Brazil de Paiva TC, Hassaan MA, Ying G-G, Huang M (2022) Detection of Neonicotinoids in agriculture soil and degradation of thiacloprid through photo degradation, biodegradation and photo-biodegradation. Environ Pollut 306:119452. https://doi.org/10.1016/j.envpol.2022.119452

Fan G, Li F, Evans DG, Duan X (2014) Catalytic applications of layered double hydroxides: recent advances and perspectives. Chem Soc Rev 43(20):7040–7066. https://doi.org/10.1039/c4cs00160e

Fatima I, Ahmad M, Vithanage M, Iqbal S (2021) Abstraction of nitrates and phosphates from water by sawdust- and rice husk-derived biochars: their potential as N- and P-loaded fertilizer for plant productivity in nutrient deficient soil. J Anal Appl Pyrol 155:105073. https://doi.org/10.1016/j.jaap.2021.105073

Gao W, Chen Y, Rao J, Hu Z, Tan Y, Wen Y, Wang Y, Zhou Z, Zhu Y, Zhou N (2022a) BCOFGs loaded with nano-FexSy for the catalytic degradation of QNC: contribution and mechanism of OFGs for reductive iron regeneration. J Hazard Mater. https://doi.org/10.1016/j.jhazmat.2022.129741

Gao W, Tan Y, Wu B, Chen Y, Hu Z, Wang Y, Wen Y, Zhou Z, Zhou N (2022b) Nano-Fe1−xS embedded BCAA/Fe3O4 as the stabilized catalyst for simultaneous quinclorac oxidation and Cr (VI) reduction. Separat Purif Technol. https://doi.org/10.1016/j.seppur.2022.121422

Guo S-P, Li J-C, Ma Z, Chi Y, Xue H-G (2016) A facile method to prepare FeS/porous carbon composite as advanced anode material for lithium-ion batteries. J Mater Sci 52(4):2345–2355. https://doi.org/10.1007/s10853-016-0527-y

Guo D, Guo Y, Huang Y, Chen Y, Dong X, Chen H, Li S (2021) Preparation and electrochemical treatment application of Ti/Sb–SnO2-Eu&rGO electrode in the degradation of clothianidin wastewater. Chemosphere. https://doi.org/10.1016/j.chemosphere.2020.129126

Guo L, Zhao L, Tang Y, Zhou J, Shi B (2022) Switching the free radical based peroxydisulfate activation to the nonradical pathway by a chrome shaving–derived biochar for the efficient degradation of tetracycline. Chem Eng J. https://doi.org/10.1016/j.cej.2022.135189

Gupta AD, Singh H, Varjani S, Awasthi MK, Giri BS, Pandey A (2022) A critical review on biochar-based catalysts for the abatement of toxic pollutants from water via advanced oxidation processes (AOPs). Sci Total Environ. https://doi.org/10.1016/j.scitotenv.2022.157831

Hirano T, Minagawa S, Furusawa Y, Yunoki T, Ikenaka Y, Yokoyama T, Hoshi N, Tabuchi Y (2019) Growth and neurite stimulating effects of the neonicotinoid pesticide clothianidin on human neuroblastoma SH-SY5Y cells. Toxicol Appl Pharmacol 383:114777. https://doi.org/10.1016/j.taap.2019.114777

Hong Q, Liu C, Wang Z, Li R, Liang X, Wang Y, Zhang Y, Song Z, Xiao Z, Cui T, Heng B, Xu B, Qi F, Ikhlaq A (2021) Electron transfer enhancing Fe (II)/Fe (III) cycle by sulfur and biochar in magnetic FeS@biochar to active peroxymonosulfate for 2,4-dichlorophenoxyacetic acid degradation. Chem Eng J 471:129238. https://doi.org/10.1016/j.cej.2021.129238

Hou J, Pugazhendhi A, Sindhu R, Vinayak V, Thanh NC, Brindhadevi K, Lan Chi NT, Yuan D (2022) An assessment of biochar as a potential amendment to enhance plant nutrient uptake. Environ Res 214:113909. https://doi.org/10.1016/j.envres.2022.113909

Huang P, Zhang P, Wang C, Du X, Jia H, Sun H (2023) P-doped biochar regulates nZVI nanocracks formation for superefficient persulfate activation. J Hazard Mater. https://doi.org/10.1016/j.jhazmat.2023.130999

Jin L, Huang Y, Ye L, Huang D, Liu X (2024) Challenges and opportunities in the selective degradation of organophosphorus herbicide glyphosate. iScience. https://doi.org/10.1016/j.isci.2024.110870

Jones A, Harrington P, Turnbull G (2014) Neonicotinoid concentrations in arable soils after seed treatment applications in preceding years. Pest Manag Sci 70(12):1780–1784. https://doi.org/10.1002/ps.3836

Kalyabina VP, Esimbekova EN, Kopylova KV, Kratasyuk VA (2021) Pesticides: formulants, distribution pathways and effects on human health—a review. Toxicol Rep 8:1179–1192. https://doi.org/10.1016/j.toxrep.2021.06.004

Lee Y-J, Lee C-G, Park S-J, Moon J-K, Alvarez PJJ (2022) pH-dependent contribution of chlorine monoxide radicals and byproducts formation during UV/chlorine treatment on clothianidin. Chem Eng J 428:132444. https://doi.org/10.1016/j.cej.2021.132444

Li L, Jiang G, Liu C, Liang H, Sun D, Li W (2012) Clothianidin dissipation in tomato and soil, and distribution in tomato peel and flesh. Food Control 25(1):265–269. https://doi.org/10.1016/j.foodcont.2011.10.046

Li H, Li S, Jin L, Lu Z, Xiang M, Wang C, Wang W, Zhang J, Li C, Xie H (2022a) Activation of peroxymonosulfate by magnetic Fe3S4/biochar composites for the efficient degradation of 2,4,6-trichlorophenol: synergistic effect and mechanism. J Environ Chem Eng 10(1):107085. https://doi.org/10.1016/j.jece.2021.107085

Li L, Yuan X, Zhou Z, Tang R, Deng Y, Huang Y, Xiong S, Su L, Zhao J, Gong D (2022b) Research progress of photocatalytic activated persulfate removal of environmental organic pollutants by metal and nonmetal based photocatalysts. J Clean Prod. https://doi.org/10.1016/j.jclepro.2022.133420

Li Y, Wang Q, Zhang X, Dong L, Yuan Y, Peng C, Zhang M, Rao P, Pervez MN, Gao N (2024) CoFe2O4/WS2 as a highly active heterogeneous catalyst for the efficient degradation of sulfathiazole by activation of peroxymonosulfate. J Water Process Eng. https://doi.org/10.1016/j.jwpe.2023.104714

Liu W, Nie C, Li W, Ao Z, Wang S, An T (2021) Oily sludge derived carbons as peroxymonosulfate activators for removing aqueous organic pollutants: performances and the key role of carbonyl groups in electron-transfer mechanism. J Hazard Mater 414:125552. https://doi.org/10.1016/j.jhazmat.2021.125552

Ma M, Xu F, Liu J, Li B, Liu Z, Gao B, Li Q (2023) Insights into S-doped iron-based carbonaceous nanocomposites with enhanced activation of persulfate for rapid degradation of organic pollutant. Chemosphere. https://doi.org/10.1016/j.chemosphere.2023.139006

Manjuri Bhuyan P, Borah S, Kumar Bhuyan B, Hazarika S, Gogoi N, Gogoi A, Gogoi P (2023) Fe3S4/biochar catalysed heterogeneous Fenton oxidation of organic contaminants: hydrogen peroxide activation and biochar enhanced reduction of Fe (III) to Fe (II). Sep Purif Technol 312:123387. https://doi.org/10.1016/j.seppur.2023.123387

Marcińczyk M, Ok YS, Oleszczuk P (2022) From waste to fertilizer: Nutrient recovery from wastewater by pristine and engineered biochars. Chemosphere. https://doi.org/10.1016/j.chemosphere.2022.135310

Mohanta D, Ahmaruzzaman M (2020) A novel Au-SnO2-rGO ternary nanoheterojunction catalyst for UV-LED induced photocatalytic degradation of clothianidin: identification of reactive intermediates, degradation pathway and in-depth mechanistic insight. J Hazard Mater. https://doi.org/10.1016/j.jhazmat.2020.122685

Nguyen Tien H, Bui DN, Manh TD, Tram NCT, Ngo VD, Mwazighe FM, Hoang HY, Le VT (2023) Electrochemical degradation of indigo carmine, P-nitrosodimethylaniline and clothianidin on a fabricated Ti/SnO2–Sb/Co-βPbO2 electrode: roles of radicals, water matrices effects and performance. Chemosphere 313:137352. https://doi.org/10.1016/j.chemosphere.2022.137352

Qi Y, Ge B, Zhang Y, Jiang B, Wang C, Akram M, Xu X (2020) Three-dimensional porous graphene-like biochar derived from Enteromorpha as a persulfate activator for sulfamethoxazole degradation: Role of graphitic N and radicals transformation. J Hazard Mater. https://doi.org/10.1016/j.jhazmat.2020.123039

Ren W, Huang X, Wang L, Liu X, Zhou Z, Wang Y, Lin C, He M, Ouyang W (2021) Degradation of simazine by heat-activated peroxydisulfate process: a coherent study on kinetics, radicals and models. Chem Eng J. https://doi.org/10.1016/j.cej.2021.131876

Sales-Alba A, Cruz-Alcalde A, López-Vinent N, Cruz L, Sans C (2023) Removal of neonicotinoid insecticide clothianidin from water by ozone-based oxidation: kinetics and transformation products. Sep Purif Technol 316:123735. https://doi.org/10.1016/j.seppur.2023.123735

Sandstrom MW, Nowell LH, Mahler BJ, Van Metre PC (2022) New-generation pesticides are prevalent in California's Central Coast streams. Sci Total Environ. https://doi.org/10.1016/j.scitotenv.2021.150683

Taghavi R, Rostamnia S, Farajzadeh M, Karimi-Maleh H, Wang J, Kim D, Jang HW, Luque R, Varma RS, Shokouhimehr M (2022) Magnetite metal-organic frameworks: applications in environmental remediation of heavy metals, organic contaminants, and other pollutants. Inorg Chem 61(40):15747–15783. https://doi.org/10.1021/acs.inorgchem.2c01939

Tian F, Qiao C, Wang C, Pang T, Guo L, Li J, Pang R, Xie H (2022) The fate of thiamethoxam and its main metabolite clothianidin in peaches and the wine-making process. Food Chem 382:132291. https://doi.org/10.1016/j.foodchem.2022.132291

Tooker JF, Pearsons KA (2021) Newer characters, same story: neonicotinoid insecticides disrupt food webs through direct and indirect effects. Curr Opin Insect Sci 46:50–56. https://doi.org/10.1016/j.cois.2021.02.013

Tu H, Wei X, Pan Y, Tang Z, Yin R, Qin J, Li H, Li AJ, Qiu R (2023) Neonicotinoid insecticides and their metabolites: Specimens tested, analytical methods and exposure characteristics in humans. J Hazard Mater. https://doi.org/10.1016/j.jhazmat.2023.131728

Wang X, Xue L, Chang S, He X, Fan T, Wu J, Niu J, Emaneghemi B (2019) Bioremediation and metabolism of clothianidin by mixed bacterial consortia enriched from contaminated soils in Chinese greenhouse. Process Biochem 78:114–122. https://doi.org/10.1016/j.procbio.2018.12.031

Wang T, Zhou Y, Xue Y, Sang T, Ren L, Chen S, Liu J, Mei M, Li J (2022) Pyrolysis of hydrothermally dewatering sewage sludge: highly efficient peroxydisulfate activation of derived biochar to degrade diclofenac. Environ Pollut 313:120176. https://doi.org/10.1016/j.envpol.2022.120176

Wang YD, Fu YW, Zhang YY, Zhao ZG, Xu T, Chen Y, Luo JY, Yang MH (2023) Residue, distribution and degradation of neonicotinoids and their metabolites in chrysanthemum plants and cultivated soils. Microchem J. https://doi.org/10.1016/j.microc.2023.109315

Wen Y, Liu M, Li S, Su L, Wang Y, Zhou Z, Zhou N, Li R (2022) Efficient removal of sulfamethazine from irrigation water using an ultra-stable magnetic carbon composite catalyst. Chem Eng J. https://doi.org/10.1016/j.cej.2022.137188

Wen Y, Liu L, He D, Wu J, Yang W, Li S, Wang S, Su L, Zhou Z, Zhou Z, Zhou N (2024) Highly graphitized biochar as nonmetallic catalyst to activate peroxymonosulfate for persistent quinclorac removal in soil through both free and non-free radical pathways. Chem Eng J. https://doi.org/10.1016/j.cej.2023.148082

Wood TJ, Goulson D (2017) The environmental risks of neonicotinoid pesticides: a review of the evidence post 2013. Environ Sci Pollut Res 24(21):17285–17325. https://doi.org/10.1007/s11356-017-9240-x

Xu W, Ni C, Deng N, Huang X (2024) Underestimated role of hydroxyl radicals for bromate formation in persulfate-based advanced oxidation processes. Environ Res. https://doi.org/10.1016/j.envres.2024.118870

Yang W, Zhao H, Chen L, Fang C, Rui Z, Yang L, Wan H, Liu J, Zhou Y, Wang P, Zou Z (2017) Ferrous sulfide-assisted hollow carbon spheres as sulfur host for advanced lithium-sulfur batteries. Chem Eng J 326:1040–1047. https://doi.org/10.1016/j.cej.2017.06.050

Yang Y, Qin S, Wang X, Cao J, Li J (2022) Dissipation behavior and acute dietary risk assessment of thiamethoxam and its metabolite clothianidin on spinach. Molecules 27(7):2209. https://doi.org/10.3390/molecules27072209

Yang W, Deng Z, Liu L, Zhou K et al (2023) Co-generation of hydroxyl and sulfate radicals via homogeneous and heterogeneous bi-catalysis with the EO-PS-EF tri-coupling system for efficient removal of refractory organic pollutants. Water Res. https://doi.org/10.1016/j.watres.2023.120312

Yu Q, Hu J, Gao Y, Gao J, Suo G, Zuo P, Wang W, Yin G (2018) Iron sulfide/carbon hybrid cluster as an anode for potassium-ion storage. J Alloy Compd 766:1086–1091. https://doi.org/10.1016/j.jallcom.2018.07.065

Yuan X, Li T, He Y, Xue N (2021) Degradation of TBBPA by nZVI activated persulfate in soil systems. Chemosphere. https://doi.org/10.1016/j.chemosphere.2021.131166

Žabar R, Komel T, Fabjan J, Kralj MB, Trebše P (2012) Photocatalytic degradation with immobilised TiO2 of three selected neonicotinoid insecticides: imidacloprid, thiamethoxam and clothianidin. Chemosphere 89(3):293–301. https://doi.org/10.1016/j.chemosphere.2012.04.039

Zhang Q, Lu Z, Chang C-H, Yu C, Wang X, Lu C (2019) Dietary risk of neonicotinoid insecticides through fruit and vegetable consumption in school-age children. Environ Int 126:672–681. https://doi.org/10.1016/j.envint.2019.02.051

Zhang C, Li F, Wen R, Zhang H, Elumalai P, Zheng Q, Chen H, Yang Y, Huang M, Ying G (2020) Heterogeneous electro–Fenton using three–dimension NZVI–BC electrodes for degradation of neonicotinoid wastewater. Water Res 182:115975. https://doi.org/10.1016/j.watres.2020.115975

Zou Z, Zhao E, Yu P, Jing J, Li Y, Li B, Wu J (2022) Simultaneous remediation of three neonicotinoids in soil using nanoscale zero-valent iron-activated persulfate process: performance, effect of process parameters, and mechanisms. Process Saf Environ Prot 167:308–321. https://doi.org/10.1016/j.psep.2022.09.005